ISSN 0915-633X

NATIONAL INSTITUTE FOR FUSION SCIENCE

Consideration of Fluctuation in Secondary Beam Intensity of Heavy Ion Beam Prove Measurements

A. Fujisawa, H. Iguchi, S. Lee and Y. Hamada

(Received - Nov. 24, 1996)

NIFS-475 Jan. 1997

RESEARCH REPORT
NIFS Series

NAGOYA, JAPAN

Consideration of Fluctuation in Secondary Beam Intensity of Heavy Ion Beam Probe Measurements

A. Fujisawa, H. Iguchi, S. Lee, Y. Hamada

National Institute for Fusion Science
Furo-cho, Chikusa-ku, Nagaya, Japan 464-01

Abstract

Heavy ion beam probes have capability to detect local electron density fluctuation in the interior of plasmas through the detected beam intensity fluctuation. However, the intensity fluctuation should suffer a certain degree of distortion from electron density and temperature fluctuations on the beam orbits, and as a result the signal can be quite different from the local density fluctuation. This paper will present a condition that the intensity fluctuation can be regarded as being purely local electron density fluctuation, together with discussion about the contamination of the fluctuation along the beam orbits to the beam intensity fluctuation.

Keywords: Heavy Ion Beam Probe, Path Integral Effect, Density Fluctuation, Temperature Fluctuation, Contamination

I. Introduction

Fluctuation induced transport in magnetically confined plasmas is one of problems to be understood for realization of a nuclear fusion reactor. The heavy ion beam probe (HIBP) is a promising tool to investigate the interior of the plasmas even in a high temperature regime[1-8]. The HIBP can measure simultaneously the plasma potential, local potential fluctuation, and 'local electron density fluctuation' through the detected beam fluctuation. The detected beam intensity varies with change of the ionization rate at the observation point, which is a function of electron density and temperature. In a sufficiently high electron temperature regime, the ionization rate shows a weak dependence on electron temperature, therefore, the beam intensity fluctuation may reflect local density fluctuation at the observation point. However, the beam intensity fluctuation should contain an integrated fluctuation of ionization rate along the beam path in the plasma (path integral effects)[9-11]. Consequently, the beam intensity does not only reflect local electron density fluctuation but also does the fluctuations occurring everywhere on beam orbits.

A number of experiments, such as in TEXT[2,3], ISX-B[4] and JIPP-TIIU[5], has been performed to investigate local density fluctuation inside of torus plasmas for the purpose of clarifying the anomalous transport. However, as is mentioned above, the fluctuation of secondary beam intensity may be 'path integrated fluctuation of the ionization cross section'. Thus, before discussing the fluctuation structure of inside plasmas using the beam intensity fluctuation, we need to answer the following questions. (i) Is the fluctuation local? (ii) Does the fluctuation purely reflect density fluctuation?

In this paper we discuss these two problems inherent with HIBP measurements, which will be also valid for other beam diagnostics. And we also would like to clarify conditions for us to regard the fluctuation as being pure density fluctuation.

II. Mathematical Preparation

II-1. Path Integration of Fluctuations

In the HIBP measurement, singly charged heavy ion beam is injected into a plasma, and the beam particle will be ionized into a doubly charged ion (secondary beam) through collisions with electrons. The secondary beam will come out from the plasma with combined information of physics quantities, such as electron density and temperature, at the birth point and on the trajectories. The secondary beam intensity is related to the primary beam

intensity, the attenuation of beam and the ionization cross-section at its birth point. And the detective secondary current $I_{\rm sec}(r)$ is described as

$$I_{\rm sec}(r) = Q_{12} I_0(r) w_{\rm s} \exp\left[-\int Q_1 {\rm d}l_1\right] \exp\left[-\int Q_2 {\rm d}l_2\right]$$

$$Q_1 = \sum_n \frac{n_e < \sigma_{1n} v_e >}{v_{\rm b}} = \sum_n \frac{n_{\rm e} S_{1n}}{v_{\rm b}} = \frac{n_{\rm e} S_1}{v_{\rm b}}$$

$$Q_2 = \sum_n \frac{n_e < \sigma_{2n} v_e >}{v_{\rm b}} = \sum_n \frac{n_{\rm e} S_{2n}}{v_{\rm b}} = \frac{n_{\rm e} S_2}{v_{\rm b}} \tag{1}$$

where $n_{\rm e}(r)$, $I_0(r)$, $v_{\rm b}$, $S_{ij} = (< \sigma_{ij} v_{\rm e} >)$ and $w_{\rm s}$ represent electron density, initial primary beam intensity, beam velocity, ionization rate form i-th to j-th states, and sample volume width, respectively, Q_1 and Q_2 and are total rate coefficients from singly and doubly charged states to higher states, respectively, and the term Q_{12} is the local brightness. These terms related to ionization rates fluctuate with variation of electron density and temperature

By differentiating Eq. (1), the beam intensity fluctuation is written as

$$\frac{\tilde{I}_{\rm sec}(r)}{I_{\rm sec}(r)} = \frac{\tilde{Q}_{12}}{Q_{12}} - \int \tilde{Q}_1 {\rm d}l - \int \tilde{Q}_2 {\rm d}l \,. \tag{2}$$

The second and third terms represent path integrated effects of fluctuations. If the condition

$$\int \tilde{Q}_1 {\rm d}l + \int \tilde{Q}_2 {\rm d}l \ll \frac{\tilde{Q}_{12}}{Q_{12}} \tag{3}$$

is satisfied, the beam fluctuation reflects local brightness fluctuation.

Next, let us consider that fluctuation amplitude in the intensity.

$$\left(\frac{\tilde{I}_{\rm sec}(r)}{I_{\rm sec}(r)}\right)^2 = T_0 + 2T_{\rm crs} + T_{\rm path}$$

$$T_0 = \left(\frac{\tilde{Q}_{12}(r)}{Q_{12}(r)}\right)^2$$

$$T_{\rm crs} = -\left(\frac{\tilde{Q}_{12}(r)}{Q_{12}(r)}\right)\left(\int \tilde{Q}_1 {\rm d}l + \int \tilde{Q}_2 {\rm d}l\right)$$

$$T_{\rm path} = \left(\int \tilde{Q}_1 {\rm d}l_1 + \int \tilde{Q}_2 {\rm d}l_2\right)^2 \tag{4}$$

where the first, the second term and the third terms are the contributions of the ionization point, of a cross talk, and of the path integrated fluctuation, respectively. The crosstalk term consists of two components,

$$T_{\rm crs}^{11} = -\frac{1}{Q_{12}} \int w_1(y)\tilde{Q}_1(x)\tilde{Q}_1(y)\mathrm{d}y,$$
$$T_{\rm crs}^{12} = -\frac{1}{Q_{12}} \int w_2(y)\tilde{Q}_1(x)\tilde{Q}_2(y)\mathrm{d}y, \tag{5}$$

and the path integration term has contributions of the following three components,

$$T_{\rm path}^{11} = \int\int w_1(x)w_1(y)\tilde{Q}_1(x)\tilde{Q}_1(y)\mathrm{d}x\mathrm{d}y,$$
$$T_{\rm path}^{12} = \int\int w_1(x)w_2(y)\tilde{Q}_1(x)\tilde{Q}_2(y)\mathrm{d}x\mathrm{d}y,$$
$$T_{\rm path}^{22} = \int\int w_2(x)w_2(y)\tilde{Q}_2(x)\tilde{Q}_2(y)\mathrm{d}x\mathrm{d}y, \tag{6}$$

where the primary and secondary trajectories are described by functions of parameters x and y, respectively, that is, $l_1 = l_1(x)$, $l_2 = l_2(y)$, and thus the term $w_i = \mathrm{d}l_i/\mathrm{d}r$ $(i = 1, 2)$ is considered to be a 'weight' in the integrals.

The terms $\tilde{Q}_{\rm i}$ are statistical variables, hence, we will consider an ensemble of fluctuations $\tilde{Q}_{\rm i}$ with $< \tilde{Q}_{\rm i} >= 0$, where $<>$ means an ensemble average. By taking the ensemble average of above formulae, we obtain

$$\left\langle \left(\frac{\tilde{I}_{\rm sec}(r)}{I_{\rm sec}(r)} \right)^2 \right\rangle =< T_0 > +2 < T_{\rm crs} > + < T_{\rm path} >$$
$$=< T_0 > +2 < T_{\rm crs}^{11} > +2 < T_{\rm crs}^{12} >$$
$$+ < T_{\rm path}^{11} > +2 < T_{\rm path}^{12} > + < T_{\rm path}^{22} >, \tag{7}$$

with the expressions of

$$< T_{\rm crs}^{ij} > = -\frac{1}{Q_{12}} \int w_i(y) < \tilde{Q}_{in}(x)\tilde{Q}_{jn}(y) > \mathrm{d}y$$
$$= -\frac{1}{Q_{12}} \int w_i(x)P_{ij}(x,\ y)\gamma_{ij}(x,\ y)\Psi_{ij}(x,\ y)\mathrm{d}y, \tag{8}$$

$$< T^{ij}_{\rm path} > = \int\int w_i(x) w_j(y) < \tilde{Q}_{1n}(x) \tilde{Q}_{1n}(y) > {\rm d}x{\rm d}y \quad (i,j=1,2)$$
$$= \int\int w_i(x) w_j(y) P_{ij}(x,\ y) \gamma_{ij}(x,\ y) \Psi_{ij}(x,\ y) {\rm d}x{\rm d}y \quad (i,j=1,2), \tag{9}$$

where $< \tilde{Q}_{ij}(x) \tilde{Q}_{lm}(y) >$ $(i,j,l,m = 1.2)$ is a correlation function of the ensemble, and $P_{\rm ij}$, γ and Ψ represent cross power, coherence and phase between fluctuations at points x and y, respectively. If we expand every term into Fourier components like $Q = \sum_\omega Q_\omega \exp(i\omega t)$ and $I_{\rm sec} = \sum_\omega I_\omega \exp(i\omega t)$, the obtained relations, Eqs. (7-9), are valid for the Fourier coefficients.

In case of micro-scale fluctuations, coherence $\gamma(x,\ y)$ should be high only when the point x is located sufficiently close to another concerning point y. On the other hand, in case of MHD fluctuations, which are expected to have a global structure, coherence $\gamma(x,\ y)$ should be high for all over the plasma, and the phase between two spatial points has a definite value. Thus, regular temporal and spatial structure of MHD fluctuation of target plasma will give significant path integral effects on the measurements.

II-2. Fluctuations in Local Ionization Coefficient

If the detected fluctuation in the secondary beam reflects pure fluctuation of local brightness, the next question is how much it represents the local density fluctuation. By taking derivatives of the local brightness function, the fluctuation of the secondary current is described as

$$\tilde{Q}_{12} = \left(\frac{\partial Q_{12}}{\partial n_{\rm e}}\right) \tilde{n}_{\rm e} + \left(\frac{\partial Q_{12}}{\partial T_{\rm e}}\right) \tilde{T}_{\rm e} = n_{\rm e} \left[\alpha_{\rm ne} \left(\frac{\tilde{n}_{\rm e}}{n_{\rm e}}\right) + \alpha_{\rm Te} \left(\frac{\tilde{T}_{\rm e}}{T_{\rm e}}\right) \right]$$
$$= n_{\rm e} \alpha_{\rm ne} \left[\left(\frac{\Delta n_{\rm e}}{n_{\rm e}}\right) + \beta \left(\frac{\Delta T_{\rm e}}{T_{\rm e}}\right) \right] , \tag{10}$$

where the coefficients are defined as

$$\alpha_{\rm Te} = T_{\rm e} \frac{\partial}{\partial T_{\rm e}} \left(\frac{S(T_{\rm e})}{v_{\rm b}}\right), \ \alpha_{\rm ne} = \frac{S(T_{\rm e})}{v_{\rm b}}, \ \beta = \frac{\alpha_{\rm Te}}{\alpha_{\rm ne}} . \tag{11}$$

By taking square of Eq. (10) as is similar to the previous section, we have

$$\tilde{Q}^2_{12} = \alpha^2_{\rm ne} n^2_{\rm e} \left[\left(\frac{\tilde{n}_{\rm e}}{n_{\rm e}}\right) + \beta \left(\frac{\tilde{T}_{\rm e}}{T_{\rm e}}\right) \right]^2 = Q^2_{12} \left[\left(\frac{\tilde{n}_{\rm e}}{n_{\rm e}}\right) + \beta \left(\frac{\tilde{T}_{\rm e}}{T_{\rm e}}\right) \right]^2 . \tag{12}$$

The ensemble average of the above expression is given by

$$\left\langle \left(\frac{\tilde{Q}_{12}}{Q_{12}}\right)^2 \right\rangle = \left\langle \left(\frac{\tilde{n}_e}{n_e}\right)^2 \right\rangle + 2\beta \left\langle \frac{\tilde{n}_e}{n_e}\frac{\tilde{T}_e}{T_e} \right\rangle + \beta^2 \left\langle \left(\frac{\tilde{T}_e}{T_e}\right)^2 \right\rangle$$
$$= \frac{P_{n_e n_e}}{n_e^2} + 2\beta \frac{P_{n_e T_e}}{n_e T_e}\gamma(n_e,\ T_e)\cos\delta(n_e,\ T_e) + \beta^2 \frac{P_{T_e T_e}}{T_e^2}\ , \tag{13}$$

where $P_{n_e n_e}$ and $P_{T_e T_e}$ represent powers of density and temperature fluctuations, respectively, and $P_{n_e T_e}$ does cross power between density and temperature fluctuations. In case that the temperature fluctuation is well correlated with the density fluctuation, the fluctuation of brightness takes a certain value between $(\tilde{n}_e + \beta\tilde{T}_e)$ and $(\tilde{n}_e - \beta\tilde{T}_e)$, which correspond to $\delta(n_e,\ T_e) = 0$ and $\delta(n_e,\ T_e) = \pi$, respectively. On the other hand, when these fluctuations are statistically independent, the flcutuation of brightness is equal to $\tilde{n}_e^2 + \beta^2\tilde{T}_e$.

III. Results from Model Calculation

We have dealt with mathematical expressions about contamination problems on the beam intensity fluctuation. In this section, we will present several calculation based on the formulae which have been derived in the previous sections. The Lotz's empirical formula[12] is used to estimate several cross sections, and we suppose that an approximation of $Q_1 \simeq Q_{12}$ and $Q_2 \simeq Q_{23}$ is valid for convenience.

III-1. Lotz's Empirical Formula

The Lotz's empirical formula gives an analytical form of the ionization rate as a function of electron temperature and electron density as follows,

$$S(T_e) = 3.0 \times 10^{-6} \sum_{i=1}^{N} \frac{\xi_i}{T_e[eV]^{1/2} I_i} \int_{I_i/T_e}^{\infty} \frac{\exp[-x]}{x} \mathrm{d}x \quad [\mathrm{cm}^3/\mathrm{s}], \tag{14}$$

where I_i and ξ_i are the ionization potential and the number of the equivalent electrons of the atom, respectively, and N means the number of the atomic shells.

One advantage of using Lotz's formula is that the contamination factor β can be expressed in a very simple form. The derivative of the rate coefficient

with respect to electron temperature is

$$\frac{\partial S(T_e)}{\partial T_e} = 3.0\times10^{-6}\sum_{i=1}^{N}\frac{\xi_i}{T_e^{3/2}I_i}\left\{\exp(-I_i/T_e) - \frac{1}{2}\int_{I_i/T_e}^{\infty}\frac{\exp[-x]}{x}\mathrm{d}x\right\} \quad [\mathrm{cm}^3/\mathrm{s}]. \tag{15}$$

Therefore, the contamination factor is expressed by

$$\beta = \alpha_{\mathrm{Te}}/\alpha_{\mathrm{ne}} = \frac{\sum_{i=1}^{N}\frac{\xi_i}{T_e^{1/2}I_i}\left\{\exp(-I_i/T_e) - \frac{1}{2}\int_{I_i/T_e}^{\infty}\frac{\exp[-x]}{x}\mathrm{d}x\right\}}{\sum_{i=1}^{N}\frac{\xi_i}{T_e^{1/2}I_i}\int_{I_i/T_e}^{\infty}\frac{\exp[-x]}{x}\mathrm{d}x}. \tag{16}$$

The ionization process from the most outer atomic shell is assumed to be dominant, then the contamination factor can be reduced into a simple form as

$$\beta = \frac{\alpha_{\mathrm{Te}}}{\alpha_{\mathrm{ne}}} = \frac{\exp(-I_{\mathrm{p}}/T_e)}{\int_{I_{\mathrm{p}}/T_e}^{\infty}\frac{\exp[-x]}{x}\mathrm{d}x} - \frac{1}{2}. \tag{17}$$

Figure 1 shows the ionization rates and the contamination factors for cesium and thallium. In case of cesium, the ionization potentials of Cs^+ and Cs^{2+} are 25.1eV, 34.6eV, respectively. The atomic structure of cesium is $[Kr][4d^{10}5s^25p^6]6s$, hence we choose 18 and 17 as the numbers of equivalent electrons for Cs^+ and Cs^{2+}, respectively. On the other hand, in case of thallium, the ionization potentials of Tl^+ and Tl^{2+} are 20.4eV, 29.8eV, respectively. The atomic structure of thallium is $[Xe][4d^{14}5d^{10}5p^6]6s^26p$, thus, the numbers of equivalent electrons are chosen to be 26 and 25 for Tl^+ and Tl^{2+}, respectively.

Figure 1b shows that the contamination factors for cesium and thallium obtained from Eq. (17). The following facts can be read from this figure. (1) In low temperature region ($T_e < 30$ eV), electron temperature fluctuation has more dominant effect on the intensity fluctuation, hence in the plasma edge region, the brightness fluctuation $\tilde{Q}_{12}$ is more sensitive to the temperature fluctuation. (2) In intermediate electron temperature region ($30 < T_e < 200$ eV), the brightness fluctuation $\tilde{Q}_{12}$ should reflect the density fluctuation more than the temperature fluctuation. (3) In high electron temperature region ($T_e > 200$ eV), the contamination factor is about 0.3, and has a negative sign. Therefore, around the plasma core region, the brightness fluctuation $\tilde{Q}_{12}$ is more sensitive to the density fluctuation.

III-2. Critical Electron Density

As beam attenuation becomes stronger, the path integral effects will be more severe. High electron density results in a strong attenuation, hence there should exist a certain critical electron density for us to regard that the detected beam fluctuation as a pure local brightness fluctuation. If we assume $\tilde{Q}_{12} = \kappa Q_{12}$, $\tilde{Q}_1 = \kappa Q_1$ and $\tilde{Q}_2 = \kappa Q_2$, the condition expressed by Eq. (3) can be reduced into the following form,

$$\Xi \equiv \int Q_1 \mathrm{d}l_1 + \int Q_2 \mathrm{d}l_2 \ll 1 \ , \tag{18}$$

where Ξ is termed here as the attenuation factor. This condition is consistent with $I_s \simeq Q_{12} I_0$, then the path integral effects should be negligible. Thus, Eq. (18) represents a condition that the intensity fluctuation reflects local fluctuation of the ionization cross section.

The integral of Eq. (18) can be modified into,

$$\int Q_1 \mathrm{d}l_1 = \bar{Q}_1 L_1 \ , \int Q_2 \mathrm{d}l_2 = \bar{Q}_2 L_2 \ , \tag{19}$$

where L_1 and L_2 are total primary and secondary path lengths, and $\bar{Q}_1$ and $\bar{Q}_2$ averages along the path. Figure 2 shows the critical electron density should satisfy

$$\Xi = \bar{Q}_1 L_1 + \bar{Q}_2 L_2 = \frac{\bar{n}_e}{v_b} \left[\bar{S}_1 L_1 + \bar{S}_2 L_2 \right] = 1 \tag{20}$$

as a function of beam energy for several average electron temperature, where $L_1 = L_2 = 0.2\mathrm{m}$ is chosen, which corresponds to a medium size plasma, and $Q_1 \simeq Q_{12}^{\mathrm{Lotz}}$ and $Q_2 \simeq Q_{23}^{\mathrm{Lotz}}$ are assumed.

III-3. Simulation of Path Integral Effects

Here, we will calculate path integrated fluctuation observed in HIBP signals on several modeled fluctuations. For simplicity, the ionization rate coefficient and length in model calculation are normalized by plasma radius a^{-1} and a, respectively. Our model plasma is assumed to have a minor radius of $a = 0.2\mathrm{m}$.

Supposed beam trajectories are shown in Fig. 3(a); in the figure the length are not normalized by plasma radius a. Using parameters s and t, these primary and secondary trajectories are described as

$$\vec{l}_1(s) = (0, \ -s+1), \ \ \vec{l}_2(t) = (t, \ -\xi t + \xi). \tag{21}$$

The corresponding weight factors are $w_1 = 1$, $w_2 = \sqrt{1+\xi^2}$. Figure 3b also demonstrates electron temperature and density profiles,

$$T_e(\rho) = 300\exp[-(\rho/0.6)^2] \ \ [\mathrm{eV}] \ .$$
$$n_e(\rho) = 1.4(1-\rho^4)^2 + 0.2 \ \ [\times 10^{13}\mathrm{cm}^{-3}]. \tag{22}$$

The cross sections are also shown in Fig. 3(c). The attenuation factors Ξ is order of 1, thus, the path integral effects will be significant in this model plasma.

The calculations are performed for density and temperature fluctuations whose distributions are expressed by $\tilde{n}_e/n_e(\rho) = \tilde{T}_e/T_e(\rho) = A\exp[-25(\rho-\rho_0)^2]$. We will treat three patterns of fluctuations, $\rho_0 = 0$, $\rho_0 = 0.5$ and $\rho_0 = 0.9$ with $A = 0.1$. These fluctuations are localized around the plasma edge (pattern A), middle of plasma radius (pattern B), and the plasma center (pattern C). Figure 4 shows radial distribution of these fluctuations, together with resulting local brightness fluctuation $\tilde{Q}/Q$. The density and temperature fluctuations have the same amplitude, and are well correlated with zero phase difference. Under these assumptions, the fluctuation of local brightness $\tilde{Q}/Q$ is enhanced by a factor $(1+\beta)$. In the fluctuation pattern localized in the plasma edge, the increase of local brightness is remarkable since the ionization rate S is strongly dependent on the electron temperature in low temperature regime.

First, we will examine dependence of the path integral effects on the coherence Ψ in Eq. (7). In calculation, the coherence is assumed to be a Gaussian form as $\gamma(x,\ y) = \exp(-l_c^{-2}|x-y|^2)$, where l_c is a correlation length, and the phase difference of the fluctuations between two spatial points $\delta(x,\ y)$ is assumed to be zero; $\Psi(x,\ y) = \cos\delta(x,\ y) = 1$. And the beam is assumed to be 50 keV cesium. Figure 5 shows intensity fluctuations of the three patterns for several correlation lengths; $l_c = 0.05$, $l_c = 0.2$, $l_c = 0.5$ and $l_c = 1.0$. The solid and dashed lines in the figures represent the amplitudes of integrated fluctuation $\tilde{I}_{\mathrm{sec}}/I_{\mathrm{sec}}$ and of original brightness fluctuation $\tilde{Q}_{12}/Q_{12}$, respectively.

In the pattern A, the points in the down stream ($\rho < 0.5$) exhibit a finite amplitude (~3-4%) due to path integration of the plasma edge fluctuation (~20%), whose absolute value is small. In this case, the contribution of T_{path} is larger than that of T_{crs}, which has a negative value. On the other hand, in the pattern C, the contribution of T_{path} is smaller than that of T_{crs}, and the amplitude in the center is smaller than that of the original brightness fluctuation. In case of $l_c = 1$, the integrated fluctuation amplitude at the

center is about a quarter (~2.5%) of the original fluctuation (~10%). In pattern B, these two effects are competing, and vary for each spatial point. As a result, the distortion is outstanding, particularly for case of $l_c = 1$, the integrated fluctuation amplitude has a completely different shape from the original one. The center value of the integrated fluctuation (~14%) is larger than the original maximum value around $\rho = 0.5$ (~10%). Generally speaking, the integrated fluctuation for every pattern tends to be flatter than the original local fluctuation, and the distortion is worse as the correlation length becomes longer.

In the above treatment, we assume that the fluctuation has no spatial structure. However, actual plasmas will have a certain mode pattern in the fluctuation, which may have a significant effect on the integrated fluctuations. Here we will consider the effect of spatial mode structure on the intensity fluctuation, concerning with the pattern B, which exhibits worst distortion in the previous calculation. Cesium beam of 50keV is assumed. The phase difference is assumed to be $\Psi(x,\ y) = \cos(m\theta)\cos(|\rho(x) - \rho(y)|\Delta\lambda^{-1})$, where θ and ρ represent between x and y and radial coordinate, respectively, and m and $\Delta\lambda$ are poloidal angle and radial periods, respectively.

Figure 6 indicates the dependence on the mode pattern for two different correlation lengths, $l_c = 1$ and $l_c = 0.1$. The case of the long correlation length is considered to correspond to MHD fluctuation. In both cases, it is observed that the integrated fluctuations $\tilde{I}_{sec}/I_{sec}$ become closer to the original brightness fluctuation distribution $\tilde{Q}_{12}/Q_{12}$ as the numbers of poloidal and radial nodes increase. This is because positive and negative spatial parts in phase pattern work to cancel out the integrals. The integrated fluctuation for $l_c = 1$ exhibits local maximums and minimums which are caused by the interference with the fluctuation mode patterns for the cases of $(\Delta\lambda,\ m) = (0.1,\ 20)$, $(\Delta\lambda,\ m) = (0.5,\ 1)$. On the other hand, the integrated fluctuation becomes monotonically closer to the local brightness fluctuation as the node number increases, since the only local structure around the ionization point can contribute to the integrals in this case.

Finally, as the beam energy increases, the interaction between beam and plasma becomes small ($\Xi \rightarrow 0$), and the contribution of path integral effects should be reduced. As is shown in Fig. 7(a), attenuation factor $\Xi(= \int Q_1 dl_1 + \int Q_2 dl_2)$ becomes small as the beam energy increases; $\Xi \propto {K_0}^{-1/2}$ is expected. The calculation of integrated fluctuation is also performed for pattern B with the assumption that correlation length of $l_c = 0.5$ and phase difference $\Psi = 1$. Figure 7(b) shows the integrated fluctuations for the beam energy of K_0 =50keV, 200keV, 1000keV. As the beam energy

increases, the integrated fluctuations are observed to become closer to the original fluctuation distribution. For case of using 1MeV beam, however, the integrated fluctuation around the center (in the down stream) still have apparent fluctuation level of 2.5%, which corresponds to about a quarter of the peak value of the original fluctuation($\sim$11%).

IV. Discussion and Summary

We have considered the fluctuation amplitude observed in secondary beam intensity. If the beam energy can be increased to a sufficiently high level, the condition of $\Xi = \int Q_1 \mathrm{d}l_1 + \int Q_2 \mathrm{d}l_2 \ll 1$ is satisfied. Then the path integral effect should become small, and the intensity signal allows us to know the phase difference of fluctuations at two points, which is another important concept. The phase difference between two adjacent spatial points has been used to estimate the wavelength for micro-scale turbulence which causes anomalous transport[2,11]. On the other hand, the intensity fluctuation is quite different from the original brightness fluctuation when the attenuation factor is large to satisfy $\Xi = \int Q_1 \mathrm{d}l_1 + \int Q_2 \mathrm{d}l_2 > 1$. The phase difference between two spatial points should be precisely known in order to reconstruct the original fluctuation amplitude (see Eqs (7-9)).

However, the phase difference from the intensity signal should suffer worse distortion than that of the amplitude when the amplitude is distorted. In cases of long correlated fluctuations, as was shown in Figs. 5(a) and (b), the fluctuation in the upper stream of trajectory can appear in its down stream, therefore, the fluctuations at two spatial points in the down stream should indicate a good correlation with nearly zero phase difference when the beam attenuation is large. In general, a condition of $|x-y| \ll l_c \ll L_{\mathrm{traj}}$ is necessary to consider that phase difference between two points is regarded as a real phase difference between two local spatial points[11], where $|x-y|$ and L_{traj} represent a distance between two spatial points, and lengths of trajectories.

The HIBP can provide local potential fluctuation in addition to the intensity fluctuation. Therefore, the original brightness fluctuation may be able to be evaluated using the phase difference between two spatial points in the potential fluctuation. The other measurements, such as Mirnov coils, soft X-ray arrays, will be also available to deduce the fluctuation mode structures.

In summary, we can regard the fluctuation in the secondary intensity as being pure local brightness fluctuation, if the beam attenuation should be sufficiently small as is expressed in Eq. (15). Moreover, the local brightness fluctuation does not reflect the density fluctuation but always does contain

electron temperature fluctuation, which can be reduced to a negligible level in sufficient high electron temperature more than several hundred eV. In case of long correlated fluctuations driven by MHD instabilities, we need to be cautious to possibilities that their regular patterns should give a cooperative effect and a large distortion on local fluctuation measurements.

References

1) F. C. Jobes, R. L. Hickok, Nucl. Fusion **10** 195(1970).

2) T. P. Crowley, P. M. Schoch, J. W. Heard, et al., Nucl. Fusion **32** 1295(1992).

3) A. Fujisawa, A. Ouroua, J. W. Heard, T. P. Crowley, et al., Nucl. Fusion **36** 375(1996).

4) G. A. Hallock, A. J. Wootton, R. L. Hickok, Phys. Rev. Lett. **59** 1301(1987).

5) Y. Hamada, A. Nishizawa, Y. Kawasumi, K. Kawahata, et al., Nucl. Fusion **36** 515(1996).

6) A. Fujisawa, H. Iguchi, S. Lee, T. P. Crowley, et al., Rev. Sci. Intrum. **67** 3099(1996).

7) K. Takasugi, H. Iguchi, M. Fujiwara and H. Ikegami. Jpn. J. Appl. Phys. **23** 364(1984).

8) J. J. Zielinski, S. C. Aceto and K. A. Connor, et al., Rev. Sci. Instrum. **59** 1822(1986).

9) D. W. Ross, M. L. Sloan, A. J. Wootton, et al., Rev. Sci. Instrum. **63** 2232(1992).

10) J. W. Heard, T. P. Crowley, D. W. Ross, et al., Rev. Sci. Instrum. **64** 1001(1993).

11) D. W. Ross, P. M. Schoch, J. W. Heard, et al., Nucl. Fusion **31** 1355(1991).

12) W. Lotz, Astophy. J. Suppl., **14** 207(1967).

Figure Captions

Fig.1: (a) Ionization rate for cesium and thallium, calculated by using the Lotz's empirical formula.(b) Contamination factor of electron temperature fluctuation for cesium and thallium cases.

Fig.2: Critical electron density as a function of beam energy in several temperature plasmas. Below this line, fluctuation in secondary intensity can be regarded as local fluctuation in local ionization cross section which is a function of electron density and temperature.

Fig.3: (a) Model of primary and secondary trajectories. (b) Assumed electron temperature and density profiles. (c) Corresponding cross sections for 50keV cesium beam.

Fig.4: Three radial distribution of assumed fluctuation pattern for density and temperature as $\tilde{n}_e/n_e = \tilde{T}_e/T_e = 0.1\exp[-25(\rho-\rho_0)^2]$ (dashed line), and the corresponding fluctuation patterns of local brightness $\tilde{Q}_{12}/Q_{12}$ (solid line). Here, we assume the electron density and temperature is well correlated, and the phase difference between them is zero.

Fig.5: Dependence of path integral effects on the coherence. The coherence is assumed to be $\gamma(x,\ y) = \exp[-l_c^{-2}|x-y|^2]$, with no phase difference between any two spatial points; $\Psi(x,\ y) = 1$. the correlation lengths are chosen to be $l_c = 0.05$, $l_c = 0.2$, $l_c = 0.5$ and $l_c = 1$. Local brightness distribution $\tilde{Q}_{12}/Q_{12}$ is indicated by the dashed line. (a) Radial distribution of intensity fluctuation for pattern A, (b) for pattern B, and (c) for pattern C. The local brightness distributions correspond to those shown in Fig. 4.

Fig.6: Dependence of path integral effects on the mode pattern of the fluctuation. The calculation is done for pattern B. The coherence and phase are assumed to be $\gamma(x,\ y) = \exp[-l_c^{-2}|x-y|^2]$ and $\Psi(x,\ y) = \cos(m\theta)\cos(|\rho(x)-\rho(y)|\Delta\lambda^{-1})$, respectively, where θ is poloidal angle between two spatial points. Local brightness distribution $\tilde{Q}_{12}/Q_{12}$ is indicated by the dashed line. Integrated fluctuation for three mode patterns, $m = 1/\Delta\lambda = 0.5$ $m = 2/\Delta\lambda = 0.25$ $m = 20/\Delta\lambda = 0.1$, with correlation lengths of (a) $l_c = 1$, (b) and $l_c = 0.1$.

Fig.7: Dependence of path integral effects on beam energy for pattern B. (a) Integrated attenuation factor $\Xi = \int Q_1 \mathrm{d}l_1 + \int Q_2 \mathrm{d}l_2$ for the beam energy K =50keV, 200keV, 1000keV. (b) Integrated fluctuation for the beam energy K =50keV, 200keV, 1000keV. In this case, $l_c = 0.5$ and $\Psi = 1.0$ are assumed. Local brightness distribution $\tilde{Q}_{12}/Q_{12}$ is indicated by the dashed line.

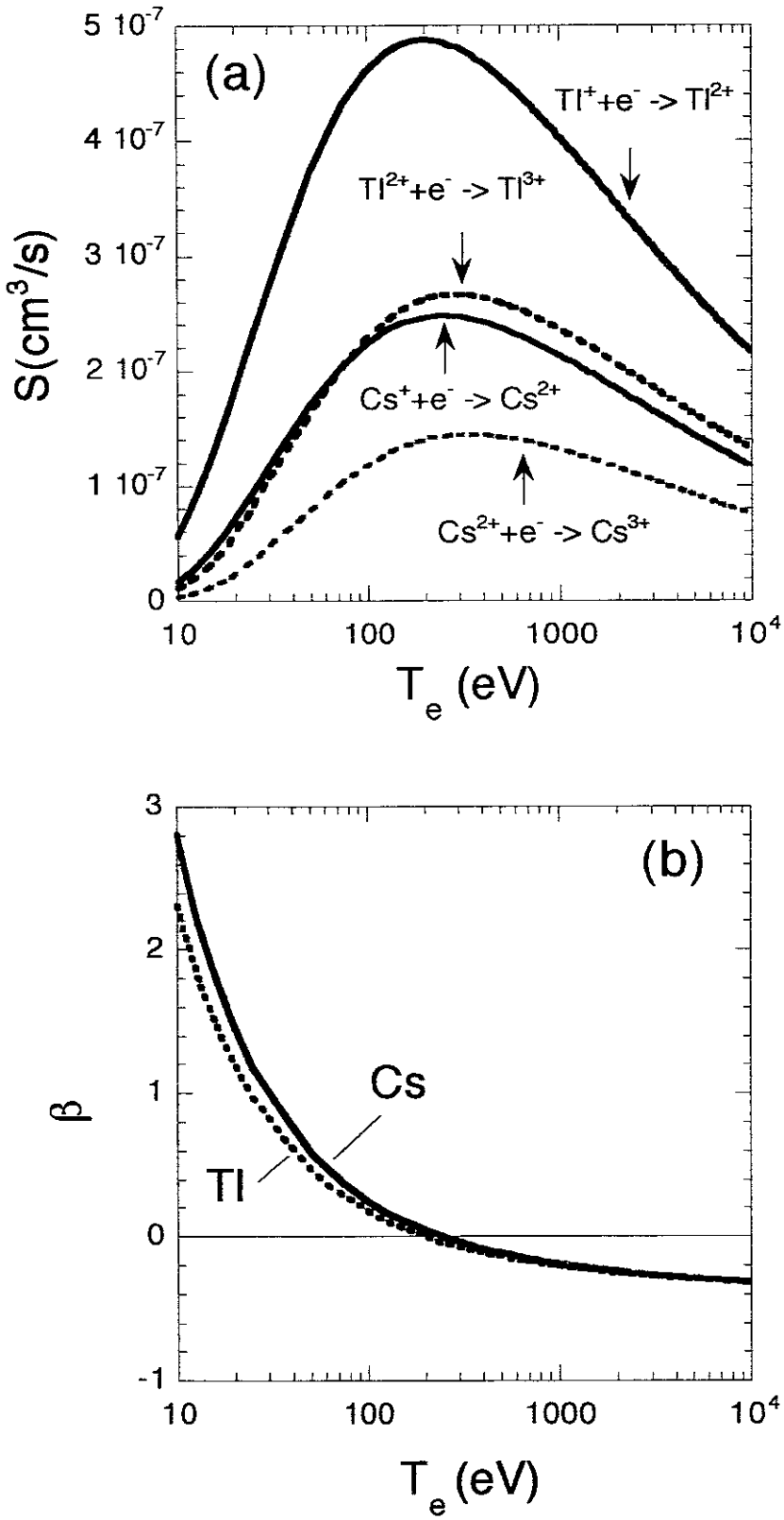

Figure 1 A. Fujisawa, et al.

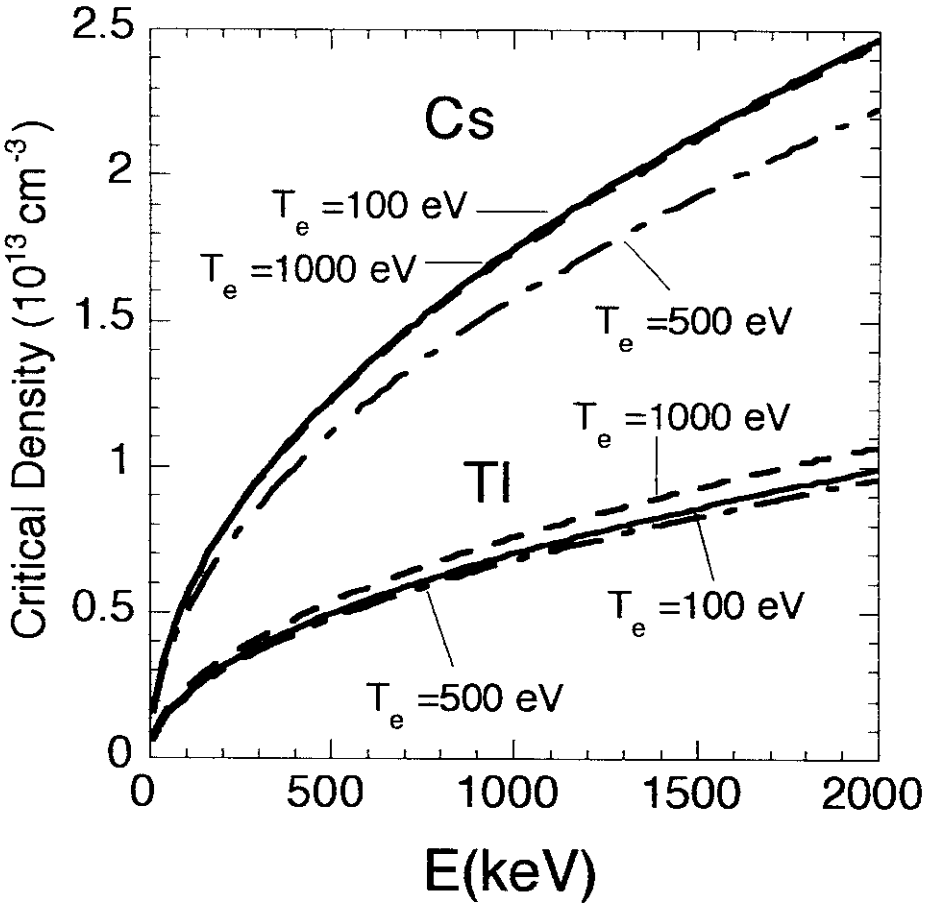

Figure 2 A. Fujisawa, et al.

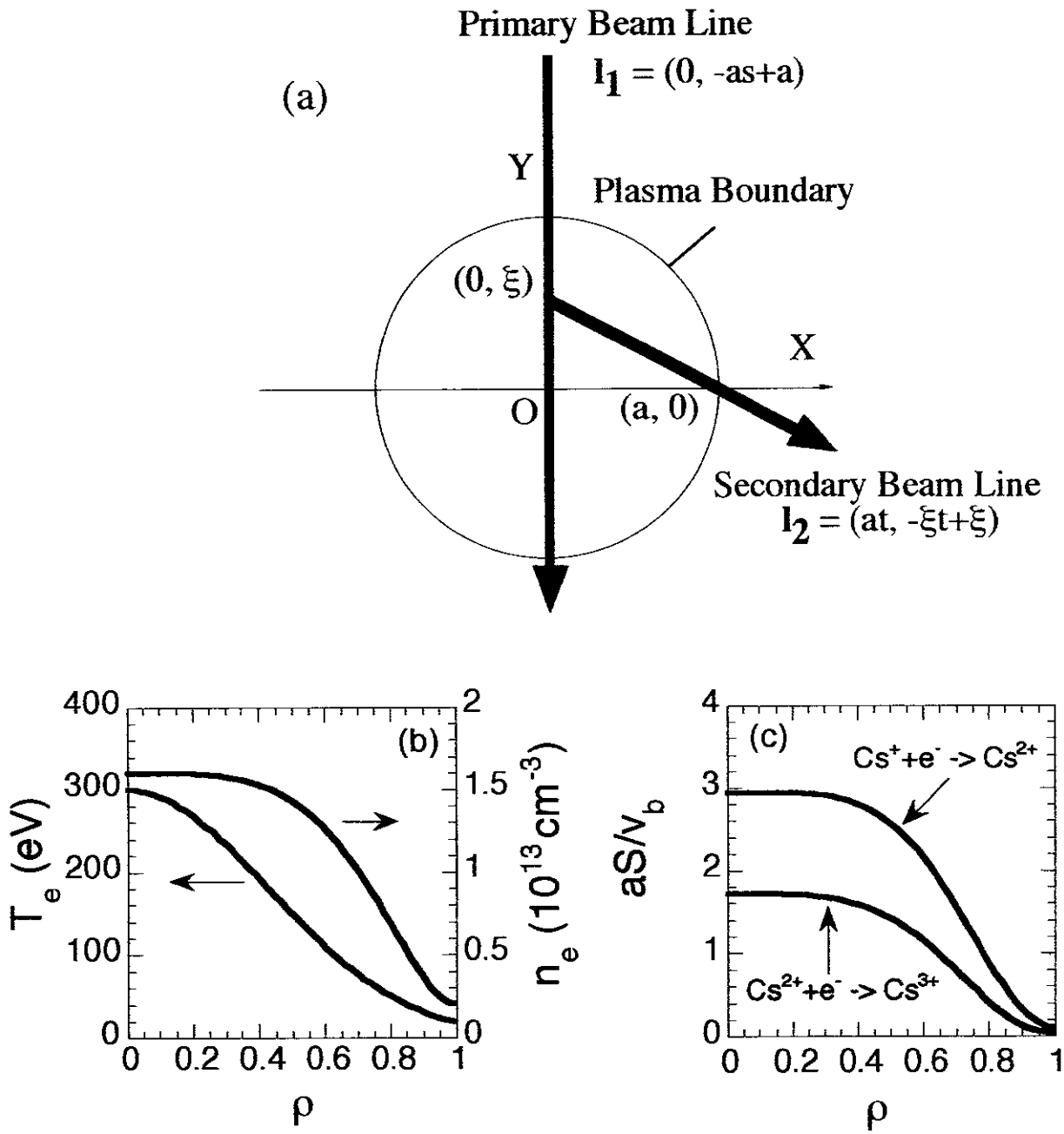

Figure 3 A. Fujisawa, et al.

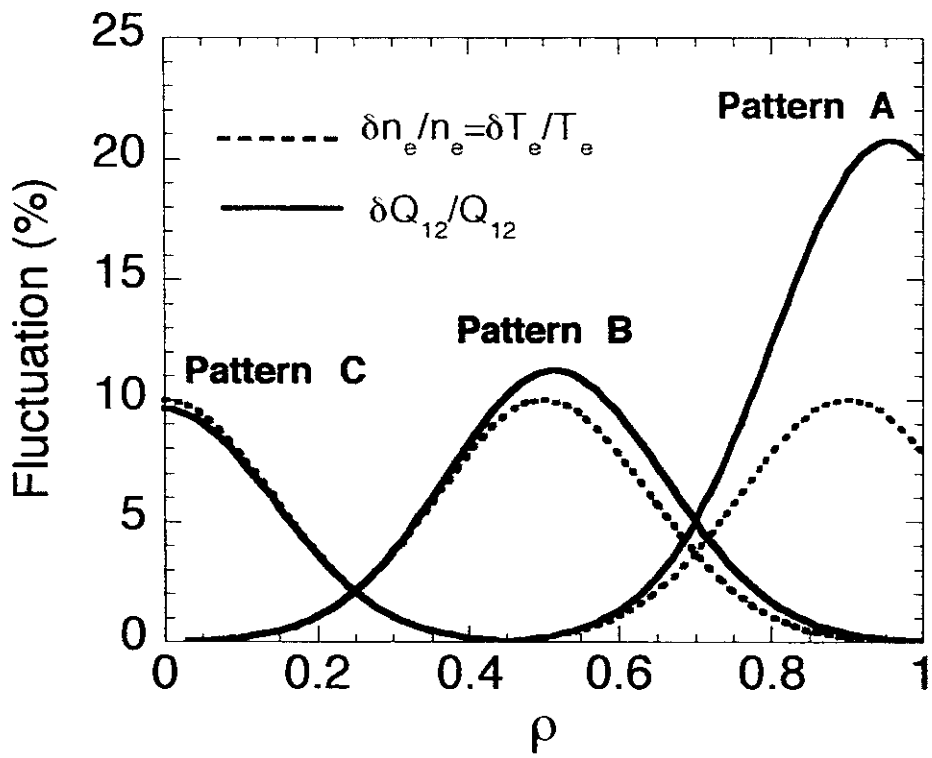

Figure 4 A. Fujisawa, et al.

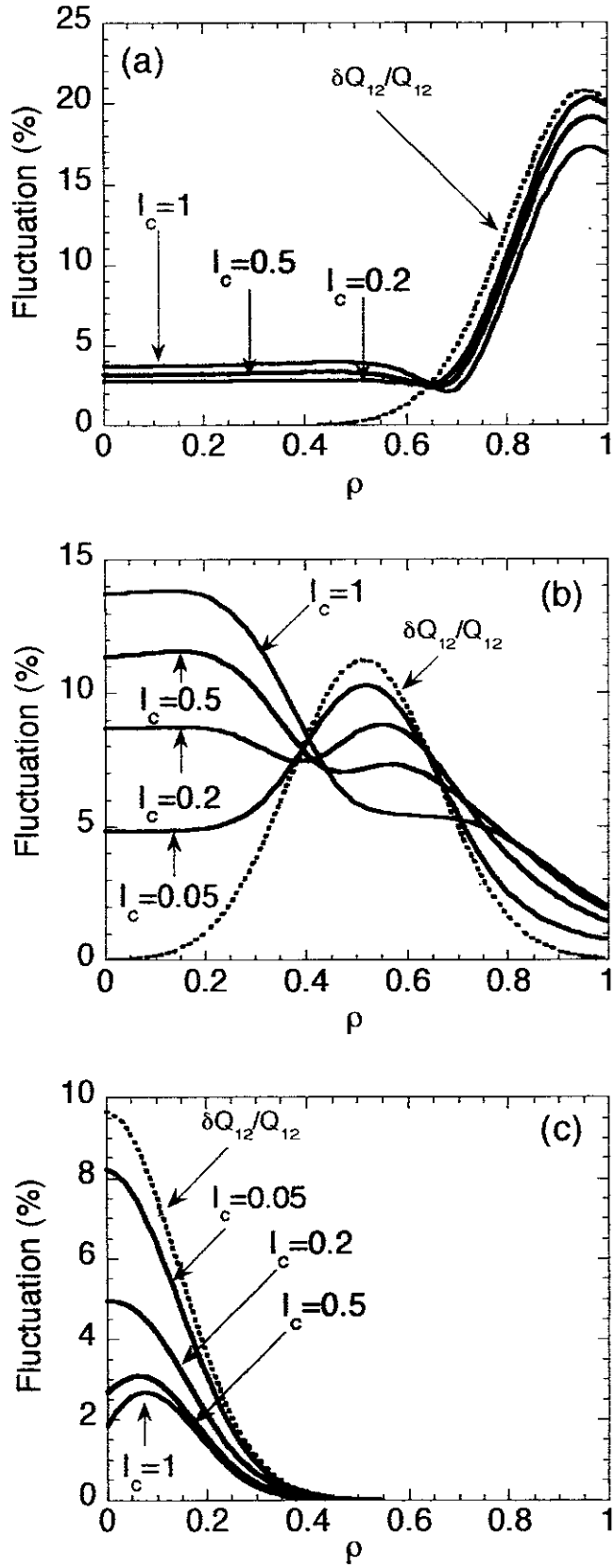

Figure 5 A. Fujisawa, et al.

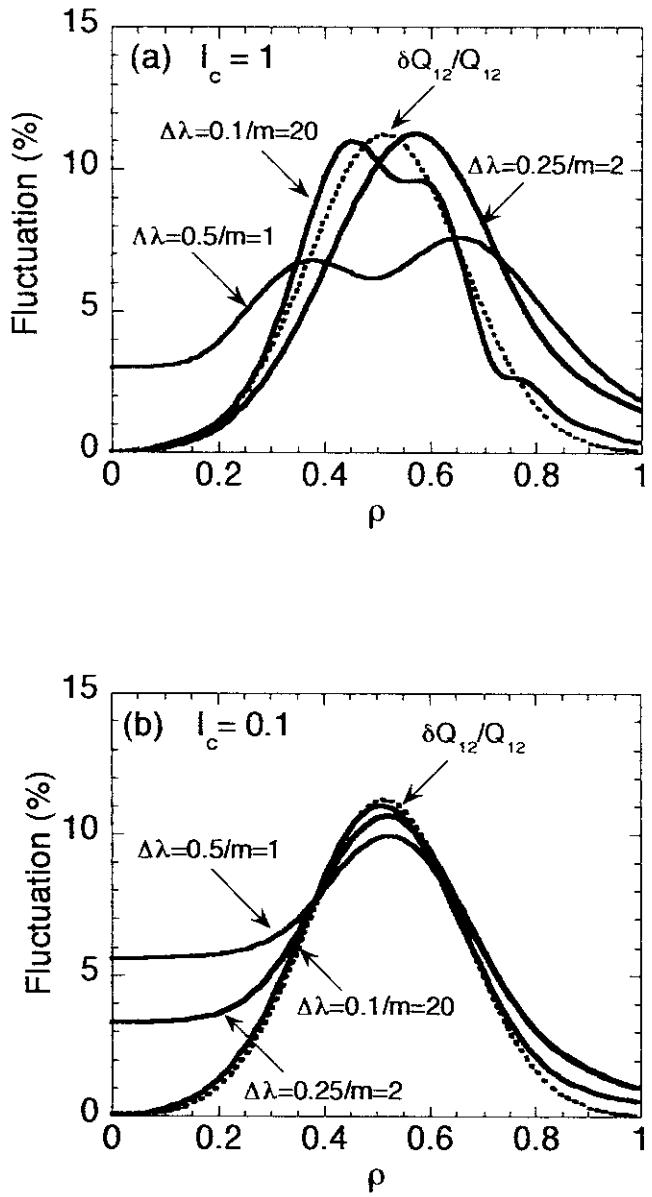

Figure 6 A. Fujisawa, et al.

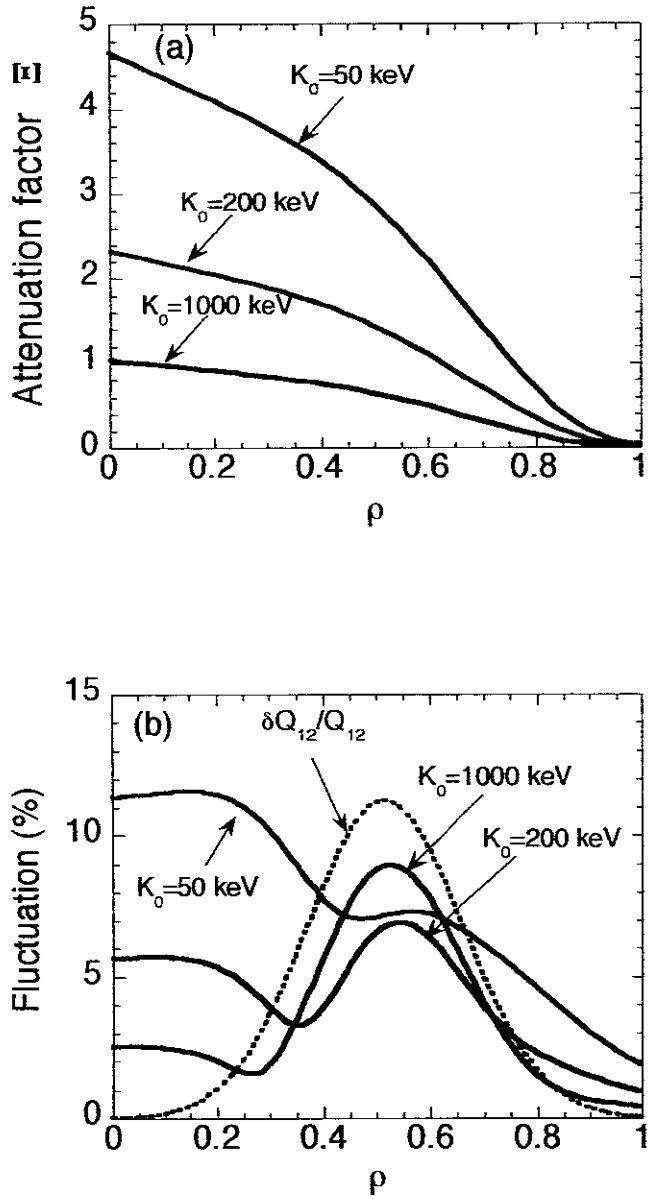

Figure 7 A. Fujisawa, et al.

Recent Issues of NIFS Series

NIFS-436 T. Kato, E. Rachlew-Källne, P. Hörling and K.-D Zastrow,
Observations and Modelling of Line Intensity Ratios of OV Multiplet Lines for 2s3s 3S1 - 2s3p 3Pj; Aug. 1996

NIFS-437 T. Morisaki, A. Komori, R. Akiyama, H. Idei, H. Iguchi, N. Inoue, Y. Kawai, S. Kubo, S. Masuzaki, K. Matsuoka, T. Minami, S. Morita, N. Noda, N. Ohyabu, S. Okamura, M. Osakabe, H. Suzuki, K. Tanaka, C. Takahashi, H. Yamada, I. Yamada and O. Motojima,
Experimental Study of Edge Plasma Structure in Various Discharges on Compact Helical System; Aug. 1996

NIFS-438 A. Komori, N. Ohyabu, S. Masuzaki, T. Morisaki, H. Suzuki, C. Takahashi, S. Sakakibara, K. Watanabe, T. Watanabe, T. Minami, S. Morita, K. Tanaka, S. Ohdachi, S. Kubo, N. Inoue, H. Yamada, K. Nishimura, S. Okamura, K. Matsuoka, O. Motojima, M. Fujiwara, A. Iiyoshi, C. C. Klepper, J.F. Lyon, A.C. England, D.E. Greenwood, D.K. Lee, D.R. Overbey, J.A. Rome, D.E. Schechter and C.T. Wilson,
Edge Plasma Control by a Local Island Divertor in the Compact Helical System; Sep. 1996 (IAEA-CN-64/C1-2)

NIFS-439 K. Ida, K. Kondo, K. Nagaski T. Hamada, H. Zushi, S. Hidekuma, F. Sano, T. Mizuuchi, H. Okada, S. Besshou, H. Funaba, Y. Kurimoto, K. Watanabe and T. Obiki,
Dynamics of Ion Temperature in Heliotron-E; Sep. 1996 (IAEA-CN-64/CP-5)

NIFS-440 S. Morita, H. Idei, H. Iguchi, S. Kubo, K. Matsuoka, T. Minami, S. Okamura, T. Ozaki, K. Tanaka, K. Toi, R. Akiyama, A. Ejiri, A. Fujisawa, M. Fujiwara, M. Goto, K. Ida, N. Inoue, A. Komori, R. Kumazawa, S. Masuzaki, T. Morisaki, S. Muto, K. Narihara, K. Nishimura, I. Nomura, S. Ohdachi, M.. Osakabe, A. Sagara, Y. Shirai, H. Suzuki, C. Takahashi, K. Tsumori, T. Watari, H. Yamada and I. Yamada,
A Study on Density Profile and Density Limit of NBI Plasmas in CHS; Sep. 1996 (IAEA-CN-64/CP-3)

NIFS-441 O. Kaneko, Y. Takeiri, K. Tsumori, Y. Oka, M. Osakabe, R. Akiyama, T. Kawamoto, E. Asano and T. Kuroda,
Development of Negative-Ion-Based Neutral Beam Injector for the Large Helical Device; Sep. 1996 (IAEA-CN-64/GP-9)

NIFS-442 K. Toi, K.N. Sato, Y. Hamada, S. Ohdachi, H. Sakakita, A. Nishizawa, A. Ejiri, K. Narihara, H. Kuramoto, Y. Kawasumi, S. Kubo, T. Seki, K. Kitachi, J. Xu, K. Ida, K. Kawahata, I. Nomura, K. Adachi, R. Akiyama, A. Fujisawa, J. Fujita, N. Hiraki, S. Hidekuma, S. Hirokura, H. Idei, T. Ido, H. Iguchi, K. Iwasaki, M. Isobe, O. Kaneko, Y. Kano, M. Kojima, J. Koog, R. Kumazawa, T. Kuroda, J. Li, R. Liang, T. Minami, S. Morita, K. Ohkubo, Y. Oka, S. Okajima, M. Osakabe, Y. Sakawa, M. Sasao, K. Sato, T. Shimpo, T. Shoji, H. Sugai, T. Watari, I. Yamada

and K. Yamauti,
Studies of Perturbative Plasma Transport, Ice Pellet Ablation and Sawtooth Phenomena in the JIPP T-IIU Tokamak; Sep. 1996 (IAEA-CN-64/A6-5)

NIFS-443 Y. Todo, T. Sato and The Complexity Simulation Group,
Vlasov-MHD and Particle-MHD Simulations of the Toroidal Alfvén Eigenmode; Sep. 1996 (IAEA-CN-64/D2-3)

NIFS-444 A. Fujisawa, S. Kubo, H. Iguchi, H. Idei, T. Minami, H. Sanuki, K. Itoh, S. Okamura, K. Matsuoka, K. Tanaka, S. Lee, M. Kojima, T.P. Crowley, Y. Hamada, M. Iwase, H. Nagasaki, H. Suzuki, N. Inoue, R. Akiyama, M. Osakabe, S. Morita, C. Takahashi, S. Muto, A. Ejiri, K. Ida, S. Nishimura, K. Narihara, I. Yamada, K. Toi, S. Ohdachi, T. Ozaki, A. Komori, K. Nishimura, S. Hidekuma, K. Ohkubo, D.A. Rasmussen, J.B. Wilgen, M. Murakami, T. Watari and M. Fujiwara,
An Experimental Study of Plasma Confinement and Heating Efficiency through the Potential Profile Measurements with a Heavy Ion Beam Probe in the Compact Helical System; Sep. 1996 (IAEA-CN-64/C1-5)

NIFS-445 O. Motojima, N. Yanagi, S. Imagawa, K. Takahata, S. Yamada, A. Iwamoto, H. Chikaraishi, S. Kitagawa, R. Maekawa, S. Masuzaki, T. Mito, T. Morisaki, A. Nishimura, S. Sakakibara, S. Satoh, T. Satow, H. Tamura, S. Tanahashi, K. Watanabe, S. Yamaguchi, J. Yamamoto, M.Fujiwara and A. Iiyoshi,
Superconducting Magnet Design and Construction of LHD; Sep. 1996 (IAEA-CN-64/G2-4)

NIFS-446 S. Murakami, N. Nakajima, S. Okamura, M. Okamoto and U. Gasparino,
Orbit Effects of Energetic Particles on the Reachable β–Value and the Radial Electric Field in NBI and ECR Heated Heliotron Plasmas; Sep. 1996 (IAEA-CN-64/CP -6) Sep. 1996

NIFS-447 K. Yamazaki, A. Sagara, O. Motojima, M. Fujiwara, T. Amano, H. Chikaraishi, S. Imagawa, T. Muroga, N. Noda, N. Ohyabu, T. Satow, J.F. Wang, K.Y. Watanabe, J. Yamamoto , H. Yamanishi, A. Kohyama, H. Matsui, O. Mitarai, T. Noda, A.A. Shishkin, S. Tanaka and T. Terai
Design Assessment of Heliotron Reactor; Sep. 1996 (IAEA-CN-64/G1-5)

NIFS-448 M. Ozaki, T. Sato and the Complexity Simulation Group,
Interactions of Convecting Magnetic Loops and Arcades; Sep. 1996

NIFS-449 T. Aoki,
Interpolated Differential Operator (IDO) Scheme for Solving Partial Differential Equations; Sep. 1996

NIFS-450 D. Biskamp and T. Sato,
Partial Reconnection in the Sawtooth Collapse; Sep. 1996

NIFS-451 J. Li, X. Gong, L. Luo, F.X. Yin, N. Noda, B. Wan, W. Xu, X. Gao, F. Yin, J.G. Jiang, Z. Wu., J.Y. Zhao, M. Wu, S. Liu and Y. Han,
Effects of High Z Probe on Plasma Behavior in HT-6M Tokamak; Sep. 1996

NIFS-452 N. Nakajima, K. Ichiguchi, M. Okamoto and R.L. Dewar,
Ballooning Modes in Heliotrons/Torsatrons; Sep. 1996 (IAEA-CN-64/D3-6)

NIFS-453 A. Iiyoshi,
Overview of Helical Systems; Sep. 1996 (IAEA-CN-64/O1-7)

NIFS-454 S. Saito, Y. Nomura, K. Hirose and Y.H. Ichikawa,
Separatrix Reconnection and Periodic Orbit Annihilation in the Harper Map; Oct. 1996

NIFS-455 K. Ichiguchi, N. Nakajima and M. Okamoto,
Topics on MHD Equilibrium and Stability in Heliotron / Torsatron; Oct. 1996

NIFS-456 G. Kawahara, S. Kida, M. Tanaka and S. Yanase,
Wrap, Tilt and Stretch of Vorticity Lines around a Strong Straight Vortex Tube in a Simple Shear Flow; Oct. 1996

NIFS-457 K. Itoh, S.- I. Itoh, A. Fukuyama and M. Yagi,
Turbulent Transport and Structural Transition in Confined Plasmas; Oct. 1996

NIFS-458 A. Kageyama and T. Sato,
Generation Mechanism of a Dipole Field by a Magnetohydrodynamic Dynamo; Oct. 1996

NIFS-459 K. Araki, J. Mizushima and S. Yanase,
The Non-axisymmetric Instability of the Wide-Gap Spherical Couette Flow; Oct. 1996

NIFS-460 Y. Hamada, A. Fujisawa, H. Iguchi, A. Nishizawa and Y. Kawasumi,
A Tandem Parallel Plate Analyzer; Nov. 1996

NIFS-461 Y. Hamada, A. Nishizawa, Y. Kawasumi, A. Fujisawa, K. Narihara, K. Ida, A. Ejiri, S. Ohdachi, K. Kawahata, K. Toi, K. Sato, T. Seki, H. Iguchi, K. Adachi, S. Hidekuma, S.Hirokura, K. Iwasaki, T. Ido, M. Kojima, J. Koong, R. Kumazawa, H. Kuramoto, T. Minami, I. Nomura, H. Sakakita, M. Sasao, K.N. Sato, T. Tsuzuki, J. Xu, I. Yamada and T. Watari,
Density Fluctuation in JIPP T-IIU Tokamak Plasmas Measured by a Heavy Ion Beam Probe; Nov. 1996

NIFS-462 N. Katsuragawa, H. Hojo and A. Mase,
Simulation Study on Cross Polarization Scattering of Ultrashort-Pulse Electromagnetic Waves; Nov. 1996

NIFS-463 V. Voitsenya, V. Konovalov, O. Motojima, K. Narihara, M. Becker and B. Schunke,
Evaluations of Different Metals for Manufacturing Mirrors of Thomson Scattering System for the LHD Divertor Plasma; Nov. 1996

NIFS-464 M. Pereyaslavets, M. Sato, T. Shimozuma, Y. Takita, H. Idei, S. Kubo, K. Ohkubo and K. Hayashi,
Development and Simulation of RF Components for High Power Millimeter Wave Gyrotrons; Nov. 1997

NIFS-465 V.S. Voitsenya, S. Masuzaki, O. Motojima, N. Noda and N. Ohyabu,
On the Use of CX Atom Analyzer for Study Characteristics of Ion Component in a LHD Divertor Plasma; Dec. 1996

NIFS-466 H. Miura and S. Kida,
Identification of Tubular Vortices in Complex Flows; Dec. 1996

NIFS-467 Y. Takeiri, Y. Oka, M. Osakabe, K. Tsumori, O. Kaneko, T. Takanashi, E. Asano, T. Kawamoto, R. Akiyama and T. Kuroda,
Suppression of Accelerated Electrons in a High-current Large Negative Ion Source; Dec. 1996

NIFS-468 A. Sagara, Y. Hasegawa, K. Tsuzuki, N. Inoue, H. Suzuki, T. Morisaki, N. Noda, O. Motojima, S. Okamura, K. Matsuoka, R. Akiyama, K. Ida, H. Idei, K. Iwasaki, S. Kubo, T. Minami, S. Morita, K. Narihara, T. Ozaki, K. Sato, C. Takahashi, K. Tanaka, K. Toi and I. Yamada,
Real Time Boronization Experiments in CHS and Scaling for LHD; Dec. 1996

NIFS-469 V.L. Vdovin, T.Watari and A. Fukuyama,
3D Maxwell-Vlasov Boundary Value Problem Solution in Stellarator Geometry in Ion Cyclotron Frequency Range (final report); Dec. 1996

NIFS-470 N. Nakajima, M. Yokoyama, M. Okamoto and J. Nührenberg,
Optimization of M=2 Stellarator; Dec. 1996

NIFS-471 A. Fujisawa, H. Iguchi, S. Lee and Y. Hamada,
Effects of Horizontal Injection Angle Displacements on Energy Measurements with Parallel Plate Energy Analyzer; Dec. 1996

NIFS-472 R. Kanno, N. Nakajima, H. Sugama, M. Okamoto and Y. Ogawa,
Effects of Finite-β and Radial Electric Fields on Neoclassical Transport in the Large Helical Device; Jan. 1997

NIFS-473 S. Murakami, N. Nakajima, U. Gasparino and M. Okamoto,
Simulation Study of Radial Electric Field in CHS and LHD; Jan. 1997

NIFS-474 K. Ohkubo, S. Kubo, H. Idei, M. Sato, T. Shimozuma and Y. Takita,
Coupling of Tilting Gaussian Beam with Hybrid Mode in the Corrugated Waveguide; Jan. 1997

NIFS-475 A. Fujisawa, H. Iguchi, S. Lee and Y. Hamada,
Consideration of Fluctuation in Secondary Beam Intensity of Heavy Ion Beam Prove Measurements; Jan. 1997